A Passively Q-Switched, CW-Pumped Fe:ZnSe Laser

Jonathan W. Evans, Patrick A. Berry, and Kenneth L. Schepler

***Abstract*— We report the demonstration of high-average-power passively Q-switched laser oscillation from Fe^{2+} ions in zinc selenide. A semiconductor saturable absorber mirror was used as a passive Q-switch element. Using a 60% R outcoupler, the pump-limited output power was 515 mW. The spectral center of the laser was 4045 nm. The pulse repetition frequency (PRF) at maximum power was ~850 kHz with a corresponding minimum pulsewidth of 64 ns Full-Width Half-Maximum. The pulse energy and peak power were >600 nJ and 8.3 W, respectively. The average output power was limited only by available pump power and increased with a slope efficiency of 22%. No thermal rolloff of slope-efficiency was observed. The beam quality was measured to be $M^2 \leq 2.6$. The temporal stability of the pulsed output was characterized. Thermal effects were shown to play a significant role in determining the PRF of the output.**

***Index Terms*— Solid-state lasers, Q-switched lasers, infrared lasers.**

I. Introduction

PULSE-AGILE solid-state infrared lasers are of interest for military, scientific, and commercial purposes including remote sensing, laser radar, and point-to-point optical communication. However, few high-power laser sources operate in the $3-5\ \mu m$ atmospheric transmission window. A notable exception is the Fe:ZnSe laser [1]–[3]. This laser material has been demonstrated to be capable of $>1\ W$ of CW output power [4] with broad tunability [5]. Fe:ZnSe lasers have been demonstrated in both continuous-wave [2], [3] and gain-switched configurations [6], [7]. However, a pulsed Fe:ZnSe laser with high average power and not requiring a pulsed pump source has not been demonstrated to date. In this work, we report the demonstration of a CW pumped high-average power passively Q-switched Fe:ZnSe laser with PRFs as high as 867 kHz with pulse widths as small as 56 ns.

II. Apparatus

Thermally-activated non-radiative processes quench the emission from Fe:ZnSe above 100 K [8]. So, for simplicity, the Fe:ZnSe crystal laser was cooled by liquid nitrogen and operated at ~77 K. As with our previous work [3], a diffusion-doped polycrystalline Fe:ZnSe sample from *IPG Photonics* with an Fe^{2+} concentration of approximately $9 \times 10^{18}\ cm^{-3}$ was used as the gain element. The Fe:ZnSe laser cavity was pumped from each end with a pair of CW Er:YAG diode-pumped solid-state (DPSS) lasers [9] with a combined maximum pump power of 3 W at 2936 nm.

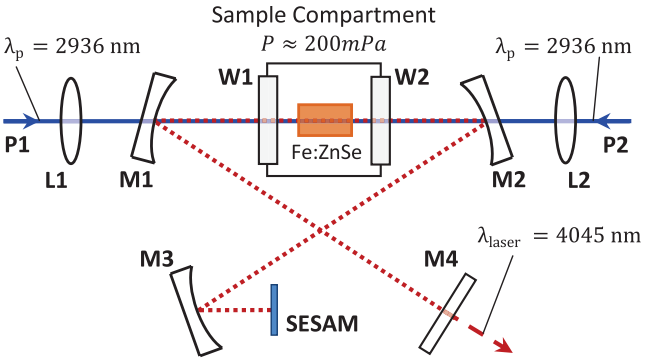

Fig. 1. A schematic view of the Fe:ZnSe laser design. All optics are made of CaF_2 and AR-coated at 2936 nm unless otherwise noted.

This work used an X-shaped cavity design with an overall length of 450 mm as shown in Fig. 1. Mirrors $M1$ and $M2$ each had an ROC of 50 mm and were placed ~100 mm from each other. This cavity geometry has the added advantage that the laser mode is roughly collimated in the crossed legs of the cavity. This collimation greatly facilitates the addition of other intracavity elements, such as a semiconductor saturable absorber mirror (SESAM). Additionally, the output of such a cavity is also nearly collimated. The beam quality of each pump beam was measured to be $M^2 \leq 2$ and each was focused through cavity mirrors into the center of the Fe:ZnSe sample. Two $f = 100\ mm$ lenses $L1$ and $L2$ were used to obtain beamwaist diameters of 210 μm. The calculated mode diameter in the cavity was 220 μm in the tangential plane and 270 μm in the sagittal plane. The Fe:ZnSe sample was $2 \times 6 \times 8\ mm^3$ and its two smallest facets were broadband AR coated from 2900 to 5000 nm. This sample was wrapped in indium foil and mounted to a copper cold-finger cooled by liquid nitrogen to ~77K. The sample compartment was evacuated to thermally insulate the Fe:ZnSe sample and the CaF_2 windows $W1$ and $W2$ were AR-coated from $2900-5000\ nm$. Mirror $M3$ had an ROC of 50 mm and focused the roughly collimated cavity mode to a small diameter on the SESAM.

The SESAM was grown by researchers at Naval Research Laboratory (NRL), and is comprised of a Bragg

Manuscript received November 1, 2013; revised December 23, 2013; accepted January 12, 2014. Date of publication January 23, 2014; date of current version February 14, 2014. This work was supported in part by the Air Force Office of Scientific Research and in part by the Sensors Directorate.

The authors are with Sensors Directorate, Air Force Research Laboratory, Wright-Patterson AFB, OH 45433 USA (e-mail: jonathan.evans@wpafb.af.mil; patrick.berry@wpafb.af.mil; kenneth.schepler@us.af.mil).

Color versions of one or more of the figures in this paper are available online at http://ieeexplore.ieee.org.

Digital Object Identifier 10.1109/JQE.2014.2302233

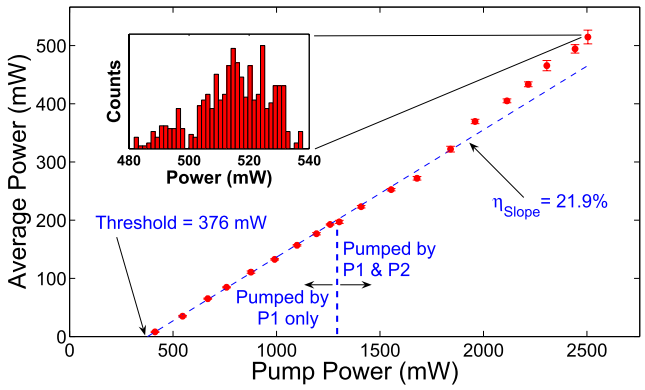

Fig. 2. The average output power of the laser with respect to the input pump power. Error bars correspond to $\pm\sigma$, the standard deviation of 500 measurements of the average power. The inset shows a histogram of the measured average output power measured at maximum pump power.

mirror, an absorbing superlattice structure and a GaSb cap. The Bragg mirror consisted of 22.5 periods of alternating GaSb/$AlAs_{0.08}Sb_{0.92}$ layers grown on a GaSb substrate (with reflectivity >99% at 4.5 μm). The absorbing superlattice was fabricated within a resonant cavity with length $2\lambda/n_{eff}$ so that the antinodes of resonance would be positioned within the absorbing region. The superlattice consisted of 129 periods of alternating InAs / $Ga_{0.92}In_{0.08}Sb$ layers with thicknesses of 23.0 Å and 27.6 Å respectively. This superlattice had an energy gap of 275 meV ($\lambda = 4.5$ μm) at room temperature and a 10 nm thick GaSb cap. The weak cavity is formed by the Bragg mirror and the interface between the air and the GaSb substrate and exhibits a fundamental mode at 4.5 μm. Simulations performed at NRL predicted that by saturating the optical absorption in the superlattice, the reflectivity from the entire structure can be modulated from ~35% to >99%. The SESAM was mounted on a linear stage so that the cavity mode size could be optimized for greatest average power. The cavity design accommodated a flat outcoupling mirror $M4$. Laser performance was evaluated for several outcouplers with different values of reflectivity.

III. Power Scaling

The operating parameters of the laser reported in this work correspond to operation with a 60% R outcoupling mirror unless otherwise indicated. In this configuration, the threshold of lasing was 376 mW and the output power increased with 22% slope efficiency with respect to coupled input power (see Fig. 2). Note that the slope efficiency suddenly increases for input power >1800 mW; we hypothesize that this is due to a change in the transverse mode profile.

With both pump lasers operating at full-power, the maximum output of the laser was measured to be 515 ± 12 mW. The greatest average power observed from this laser was 627 mW and was achieved using a 44% R outcoupling mirror. However, the trends of Figs. 2 and 4 exhibited substantially more variation in this configuration.

The values of input power shown on Fig. 2 are direct measurements of the power incident on the windows to the sample compartment. Spectral scans of the output with a monochromator show no content at the pump wavelength. The threshold and slope efficiency of the laser were extracted as fit parameters from a least-squares fit of a linear model to the average output power data plotted against input power. Table I shows the pump power at the threshold of lasing, the maximum average power, and the slope efficiency of the laser using 44%, 60%, 71%, 90% and 94% reflective output coupling mirrors. The slope efficiency of the laser clearly increased with respect to the transmission of the outcoupling mirror. The threshold of lasing was relatively insensitive to the transmission of the outcoupling mirror, no more than an 80 mW increase in the threshold power resulting from a two-fold increase in the transmission of the outcoupling mirror.

TABLE I
THE INPUT/OUTPUT POWER CHARACTERISTICS OF THE LASER WITH VARYING OUTCOUPLER MIRRORS

Outcoupler (% R)	Threshold (mW)	Max. Power (mW)	η_{slope}
44	350	627 ± 12	29%
60	376	515 ± 12	22%
71	293	395 ± 6	18%
90	252	184 ± 3	8.0%
94	291	111 ± 2	5.0%

From the inset histogram of Fig. 2 we see that the average power of the laser output exhibited some variation. The coefficient of variation of the laser power was $C_v(P) = \sigma_{Power}/\mu_{Power}$ where σ_{Power} is the standard deviation of the average power and μ_{Power} is its mean. Neither the addition of a 25 μm Si etalon nor an adjustable iris within the laser cavity significantly affected the power stability $C_v(P)$ of the laser output. The SESAM was replaced with an HR dielectric mirror to force the laser to operate in the continuous wave regime. The measured instability was not significantly affected, however, the threshold of the laser fell by 12% and the slope efficiency increased by a factor of 1.6. These observations confirm that passive losses of the first-generation unoptimized SESAM are significant but that the use of the SESAM does not produce the observed variation in average power. Moreover, visually inspection showed no evidence of optically-induced damage to the SESAM.

IV. Temporal Characteristics

The first Q-switched Cr:ZnSe laser was demonstrated in 2003 by Alford et al. [10] using an RTP Pockels cell to actively modulate the quality factor Q of the laser cavity. In 2005, Pollock et al. [11] demonstrated a pulsed Cr:ZnSe laser using a SESAM as a passive Q-switch. Similarly the Fe:ZnSe laser demonstrated in this work used a SESAM as a passive Q-switch to realize pulsed output (see Fig. 3) using a CW pump.

The period T between output pulses is the time required for the intracavity radiation to grow to the saturation intensity of the SESAM. The rate of growth of the intracavity intensity is determined primarily by the outcoupler reflectivity and the input power from the pump laser(s). Thus the pulse repetition

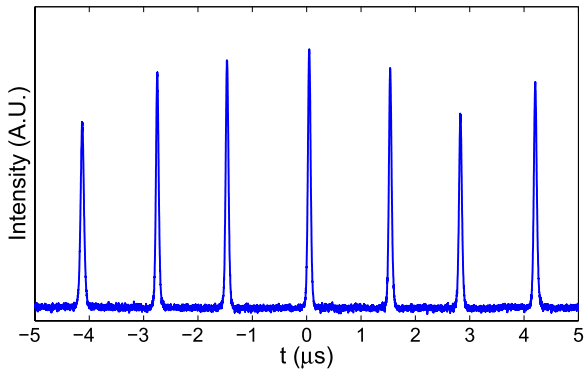

Fig. 3. The output of the laser using a 60% R outcoupling mirror and operating at maximum power. The trace was captured using a 2 GHz oscilloscope and a *VIGO PVM-10.6* photodiode with a 1.5 ns response time.

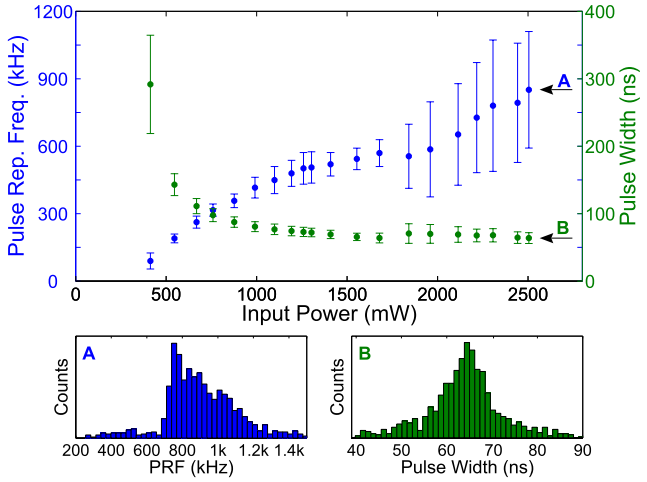

Fig. 4. The temporal pulse characteristics of the laser with respect to the input pump power. Data points correspond to the mean of 1000 samples of the observed quantity and error bars correspond to $\pm\sigma$, the standard deviation of the observed quantity. The histograms show the statistical behavior of pulse characteristics at full power as indicated.

frequency $F = 1/T$ of the laser could be varied greatly by adjusting these parameters. T was measured as the average of 1000 time intervals between consecutive pulses as recorded by an oscilloscope with a fast photodiode. The PRF was observed to increase with pump power as shown in Fig. 4. Note that the PRF trend exhibits a shift at 1800 mW of pump power; we hypothesize that this shift, like the jump in the output power at the same value of pump power, is due to a change in the transverse mode profile.

The increasing trend in PRF with respect to pump power was initially linear for all outcouplers. For each outcoupler, the trend rolled off with increasing pump power. Spühler et al. have shown that this trend should be strictly linear [12], so it was hypothesized that the deviation with increased power was due to thermal effects in the Fe:ZnSe crystal.

The variation in the pulse-to-pulse arrival time was found to increase with the input pump power. The coefficient of variation for T can be calculated $C_v(T) = \sigma_T/\mu_T$ where σ_T is the standard deviation of the pulse-to-pulse arrival and μ_T is its mean. Both the addition of a 25 μm Si etalon and the

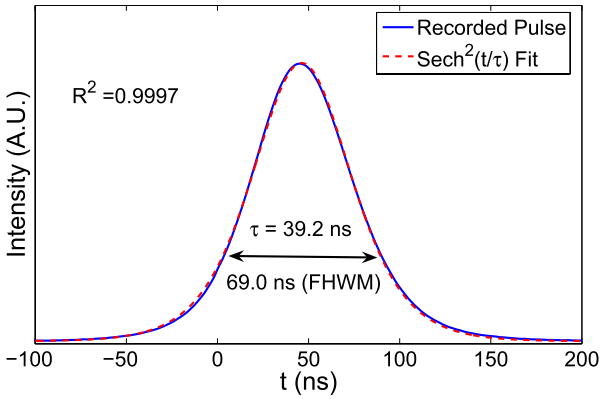

Fig. 5. A time-average of 1000 pulses from the laser at maximum power. The numerical fit (dashed red line) of a hyperbolic secant distribution exhibits excellent agreement with the recorded average pulse (solid blue line).

addition of an adjustable iris within the laser cavity resulted in an increase in $C_v(T)$.

The pulse width of the output pulses was measured by recording the time average of 1000 pulses as shown in Fig. 5. The width 2τ of the average pulse was extracted from a numerical fit of the hyperbolic secant squared pulse-shape

$$I(t) = A \cdot sech^2\left(\frac{t - t_0}{\tau}\right) + a$$

to the time-averaged pulse. It can be shown that the Full-Width Half-Maximum (FWHM) pulse width of a secant-squared shaped pulse can be calculated as $W_{FWHM} = 0.8814 \cdot 2\tau$. All pulse widths reported in this work are FWHM values determined in this manner.

For all outcouplers, the width of the average pulse decreased with respect to pump power and asymptotically approached some limiting value (see Fig. 4). The pulse width was 64 ns at maximum pump power for the 60% R outcoupler. The minimum pulse width observed was 56 ns at maximum pump power using a 94% R outcoupling mirror. Spühler et al. have shown that the pulse width of a SESAM Q-switched laser should be insensitive to the pump power. However, they also demonstrated a Nd:YVO_4 SESAM Q-switched laser for which the pulse width is considerably larger than the limiting value near threshold. They ascribed this behavior to terms neglected in their theoretical analysis [12], though it is not clear that these terms were responsible for the similar behavior observed in this work.

It can be shown that, for a hyperbolic secant-squared shaped pulse, the pulse energy of the average pulse can be directly calculated $P_{peak} = PT/2\tau$ where P is the average power, T is the average period between pulses, and 2τ is the the average pulse width. Using the 60% R outcoupler, the maximum average power value was 515 mW at a PRF of 851 kHz. The pulse width $2\tau = 72.3$ ns implies a pulse energy of 605 nJ and a peak power of 8.3 W, substantially greater than the average value of power. Table II shows the operating characteristics of the output of the laser using 44%, 60%, 71%, 90% and 94% R reflective output coupling mirrors.

Fig. 6 shows the increase of pulse energy and peak power with increased pump power. Note that the instability of the

TABLE II
THE TEMPORAL CHARACTERISTICS OF THE LASER PULSES WITH VARYING OUTCOUPLER MIRRORS AT MAXIMUM PUMP POWER

Outcoupling Mirror (% R)	PRF (kHz)	Pulse Width (ns)	Peak Power (W)	Pulse Energy (nJ)
44	867 ± 266	64.5 ± 26.8	8.9 ± 3.5	651 ± 201
60	851 ± 260	63.7 ± 10.3	8.3 ± 2.7	605 ± 185
71	766 ± 159	63.5 ± 10.6	7.2 ± 2.6	521 ± 109
90	712 ± 174	62.6 ± 8.9	3.7 ± 1.3	261 ± 64
94	683 ± 127	56.1 ± 7.5	2.3 ± 0.7	147 ± 27

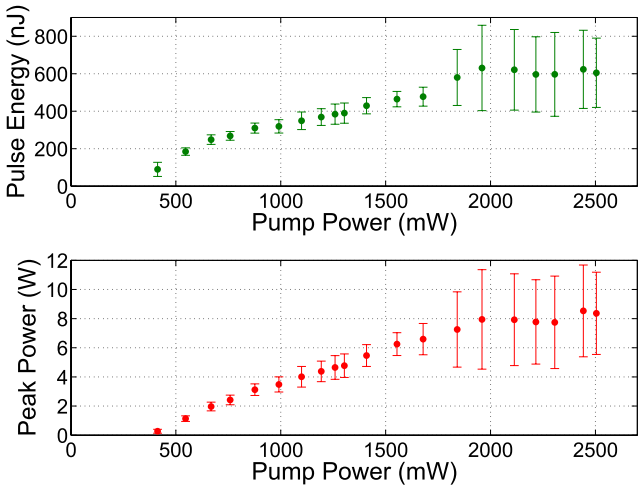

Fig. 6. The average pulse energy and peak power of the laser with respect to pump power.

laser increases substantially with increasing pump power. Again we note an abrupt change in the behavior at 1800 mW of pump power. The variation in the peak power and pulse energy calculation are derived from the variation of the pulse-to-pulse period seen in Fig. 4.

V. THERMAL EFFECTS

Recall that Figs. 2, 4, and 6 exhibit behavior consistent with a sudden change of the transverse mode of the laser cavity at a pump power of 1800 mW. We have hypothesized that this is due to thermal effects induced in the gain medium by the pump laser. To test this hypothesis, the laser cavity was operated with pump laser $P1$ at full power and $P2$ off. The pulse width and repetition frequency were observed both with $P1$ free-running and with $P1$ chopped by a 50% duty-cycle chopper wheel at $\sim$150 Hz. The instantaneous pump power is identical in both cases, and the chopping time is much longer than the temporal pulse width of the laser, so the laser dynamics should be identical in both cases. However, the thermal load on the cooling system in the continuously illuminated case is twice that of the chopped case. Thus, thermal lensing is more severe. The result of this lensing is a change of the mode size of the cavity mode on the SESAM, and thus a change in the amount of time it takes for the absorption to saturate. Thus, these two configurations exhibit different pulse behavior as seen in Fig. 7.

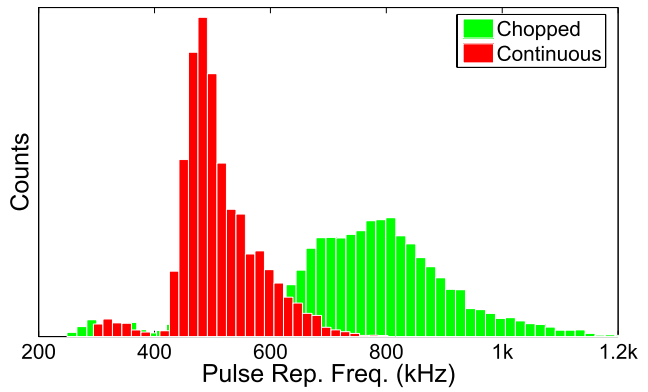

Fig. 7. The histograms of pulse repetition frequency of the laser output with $P2$ off and with (green) and without (red) $P1$ chopped at a 50% duty cycle.

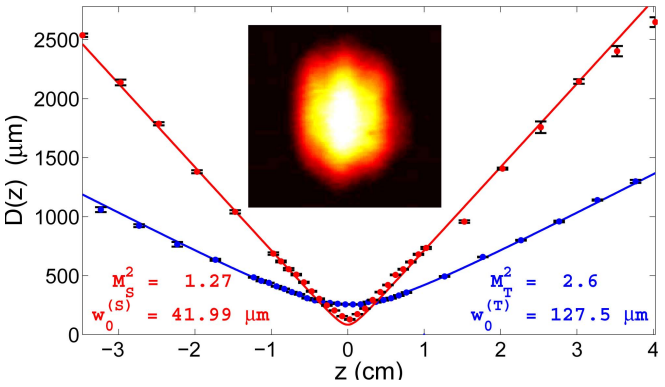

Fig. 8. Beam profile of the Fe:ZnSe laser operating at maximum power. The inset is a picture of the beam as recorded by an *Electrophysics PV320* beamprofiling camera.

VI. BEAM QUALITY

To measure the beam quality of the laser, the output of the Fe:ZnSe laser was focused using a 75 mm lens. The beamwidth $w(z)$ of the focused beam was measured using the second moments definition. Measurements were taken at evenly spaced locations along the optic axis using a *Photon Inc. Nanoscan* scanning slit beam profiling tool. The beam quality M^2 and the beamwaist radius w_0 were determined as parameters of a least-squares fit to the beam width data of the Gaussian beam propagation formula

$$w(z) = w_0 \cdot \sqrt{1 + M^2 \left(\frac{z}{z_R}\right)^2}$$

where z_R is the Rayleigh range of the beam, w_0 is the beamwaist and the zero of z is defined at the beamwaist. Fig. 8 shows the profile of the output beam. When pumping with both $P1$ and $P2$ at full power the beam quality was measured to be $M_S^2 = 1.27$ and $M_T^2 = 2.60$. This astigmatism was expected as a consequence of a non-zero angle of incidence of the cavity mode on the curved mirrors $M1$ and $M2$.

VII. SPECTRAL CONTENT

The output of the laser, both at threshold and at full power, was spectrally resolved using an *Acton SpectraPro-300*

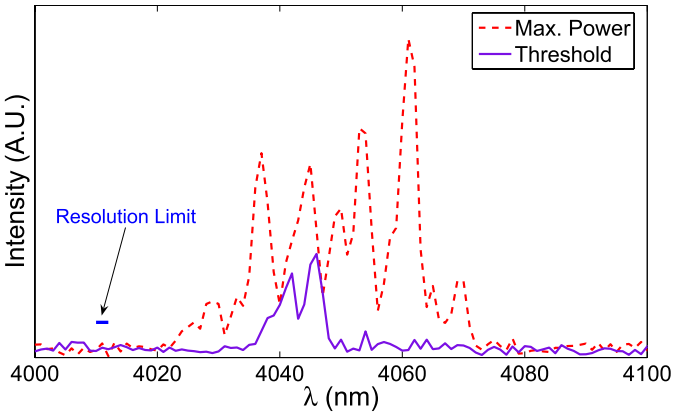

Fig. 9. The emission spectra of the Fe:ZnSe laser operating at threshold (solid) and at maximum average power (dashed). The structure in the output is consistent with behavior observed in our CW Fe:ZnSe laser work (see [3]) that was theorized to be evidence of mode-hopping.

monochromator with a liquid nitrogen cooled InSb detector. The instrument used a 1.5″ effective grating diameter with 300 gr/mm blazed at 2 μm. The slits were set to 100 μm, so the the wavelength resolution was < 2 nm. Fig. 9 shows the time average emission spectra of the laser at threshold and maximum power. The threshold output wavelength of 4045 nm varies slightly from the calculated peak gain wavelength of 4075 nm and varies substantially from the 4140 nm reported in our CW Fe:ZnSe laser work [3], but is consistent with other free-running Fe:ZnSe lasers [2]. Such variations in spectral output wavelength are due to spectral differences in the reflectivity of the cavity mirror coatings as well as the spectral losses introduced by the SESAM. Clearly, the spectral width of the output increases with pump power. The structure observed in the output spectrum was also observed in our CW work and was found to be a consequence of time averaging. The individual peaks were not simultaneously present in the output. A linear array on the output of a monochromator allowed real-time monitoring of the output spectrum and the CW laser was observed to rapidly switch between operation at several wavelengths. Time-resolved spectroscopic monitoring of the output of the Q-switched laser was not attempted, though the structure in the time-averaged output spectrum is consistent with mode-hopping.

VIII. Conclusion

In conclusion, we have demonstrated >0.6 W of Q-switched output power at PRFs >850 kHz from a CW-pumped Fe:ZnSe laser. The temporal characteristics of the output pulse train were demonstrated to vary greatly with respect to the average output power. The minimum pulse width measured from the laser was 56 ns. The output wavelength of the laser exhibited some variation but was centered at 4045 nm and the beam quality was $M^2 < 2.60$. Neglecting coupling losses, the maximum achieved optical efficiency of the laser was 25% at full power. The average output power of the laser was only limited by the available pump power. The pulse-width and the PRF of the output were observed to depend directly on the input power. Significant deviations from the trends predicted by Spühler et al. for were observed for these quantities and evidence was presented that thermal effects significantly affect the pulse repetition rate of the laser.

Acknowledgment

We thank Jerry Meyer and Igor Vurgaftman of NRL for fabrication of the SESAM.

References

[1] J. J. Adams, C. Bibeau, R. H. Page, and S. A. Payne, "Tunable laser action at 4.0 microns from Fe:ZnSe," in *Proc. ASSL*, Jan. 1999, no. WD3, pp. 1–3.

[2] A. A. Voronov, V. I. Kozlovskii, Y. V. Korostelin, A. I. Landman, Y. P. Podmar'kov, Y. K. Skasyrskii, *et al.*, "A continuous-wave Fe^{2+}:ZnSe laser," *Quantum Electron.*, vol. 38, no. 12, pp. 1113–1116, 2008.

[3] J. W. Evans, P. A. Berry, and K. L. Schepler, "840 mW continuous-wave Fe:ZnSe laser operating at 4140 nm," *Opt. Lett.*, vol. 37, no. 23, pp. 5021–5023, Dec. 2012.

[4] V. Fedorov, D. Martyshkin, M. Mirov, I. S. Moskalev, S. Vasilyev, J. Peppers, *et al.*, "Fe-doped II–VI mid-infrared laser materials for the 3 to 8 μm Region," in *Proc. CLEO*, Jun. 2013, no. JM4K.2, pp. 1–3.

[5] J. W. Evans, P. A. Berry, and K. L. Schepler, "A broadly tunable continuous-wave Fe:ZnSe laser," *Proc. SPIE*, vol. 8599, no. 11, pp. 85990C-1–85990C-8, Mar. 2013.

[6] J. J. Adams, C. Bibeau, R. H. Page, D. M. Krol, L. H. Furu, and S. A. Payne, "4.0–4.5 μm lasing of Fe:ZnSe below 180 K, a new mid-infrared laser material," *Opt. Lett.*, vol. 24, no. 23, pp. 1720–1722, Dec. 1999.

[7] A. A. Voronov, V. I. Kozlovskii, Y. V. Korostelin, A. I. Landman, Y. P. Podmar'kov, and M. P. Frolov, "Laser parameters of a Fe:ZnSe crystal in the 85–255 K temperature range," *Quantum Electron.*, vol. 35, no. 9, pp. 809–812, 2005.

[8] N. Myoung, V. V. Fedorov, S. B. Mirov, and L. E. Wenger, "Temperature and concentration quenching of mid-IR photoluminescence in iron doped ZnSe and ZnS laser crystals," *J. Lumin.*, vol. 132, no. 3, pp. 600–606, Mar. 2012.

[9] J. G. Sousa, D. Welford, and J. Foster, "Efficient 1.5 W CW and 7 mJ quasi-CW TEM_{00} mode operation of a compact diode-laser pumped 2.94 μm Er:YAG laser," *Proc. SPIE*, vol. 7578, pp. 75781E-1–75781E-8, Feb. 2010.

[10] W. J. Alford, G. J. Wagner, A. C. Sullivan, J. A. Keene, and T. J. Carrig, "High-power and Q-switched Cr:ZnSe lasers," in *Proc. ASSP*, Feb. 2003, p. 13.

[11] C. R. Pollock, N. A. Brilliant, D. Gwin, T. J. Carrig, W. J. Alford, J. B. Heroux, *et al.*, "Mode locked and Q-switched Cr:ZnSe laser using a semiconductor saturable absorbing mirror," in *Proc. ASSP*, Feb. 2005, p. 252.

[12] G. J. Spühler, R. Paschotta, R. Fluck, B. Braun, M. Moser, G. Zhang, *et al.*, "Experimentally confirmed design guidelines for passively Q-switched microchip lasers using semiconductor saturable absorbers," *J. Opt. Soc. Amer. B, Opt. Phys.*, vol. 16, no. 3, pp. 376–388, Mar. 1999.

Jonathan W. Evans received the B.S. degree in electrical engineering from Cedarville University in 2008, the M.S. degree in electro-optics from The University of Dayton in 2010, and the Ph.D. degree in optical sciences and engineering from the Air Force Institute of Technology in 2014. He joined the Air Force Research Laboratory as a Civilian at Wright-Patterson Air Force Base, Ohio, in 2008. He is currently an Optical Engineer with the Sensors Directorate of the Air Force Research Laboratory. His interests include solid state lasers, infrared spectroscopy, and nonlinear frequency conversion. He is a member of the Optical Society of America.

Patrick A. Berry received the B.S. degree in chemistry and physics from the University of Wisconsin – La Crosse in 2003, and the M.S. and Ph.D. degrees in electro-optics from the University of Dayton, Dayton, OH, USA, in 2005 and 2010, respectively. He works in laser source development for the Sensors Directorate of the U.S. Air Force Research Laboratory. His research interests are in high power versatile laser sources for the mid-IR region.

Kenneth L. Schepler received the B.S. degree in physics from Michigan State University in 1971 and the Ph.D. degree in physics from The University of Michigan in 1975. He joined the Avionics Laboratory as a Civilian at Wright-Patterson Air Force Base, Ohio in 1981. He is currently a Principal Research Physicist with the Sensors Directorate of the Air Force Research Laboratory. His interests include solid state laser physics, laser materials spectroscopy, and nonlinear frequency conversion. He is a fellow of the Optical Society of America and the Air Force Research Laboratory.